Dynamic Response of a Clamped Circular Sandwich Plate Subject to Shock Loading

X. Qiu

V. S. Deshpande

N. A. Fleck[1]
e-mail: naf1@eng.cam.ac.uk

Engineering Department,
Cambridge University,
Trumpington Street,
Cambridge CB1 1PZ, UK

An analytical model is developed for the deformation response of clamped circular sandwich plates subjected to shock loading in air and in water. The deformation history is divided into three sequential stages and analytical expressions are derived for the deflection, degree of core compression, and for the overall structural response time. An explicit finite element method is employed to assess the accuracy of the analytical formulas for the simplified case where the effects of fluid-structure interaction are neglected. The sandwich panel response has only a low sensitivity to the magnitude of the core compressive strength and to the degree of strain hardening in the face-sheets. The finite element results confirm the accuracy of the analytical predictions for the rigid ideally plastic sandwich plates. The analytical formulas are employed to determine optimal geometries of the sandwich plates that maximize the shock resistance of the plates for a given mass. The optimization reveals that sandwich plates have a superior shock resistance relative to monolithic plates of the same mass. [DOI: 10.1115/1.1778416]

1 Introduction

Clamped sandwich plates are representative of the structures used in the design of commercial and military vehicles. For example, the outermost structure on a ship comprises plates welded to an array of stiffeners. The superior performance of sandwich plates relative to monolithic solid plates is well known for applications requiring high quasi-static strength. However, the resistance of sandwich plates to dynamic loads remains to be fully investigated in order to quantify the advantages of sandwich design over monolithic design for application in shock resistant structures.

The response of monolithic beams and plates to shock type loading has been extensively investigated over the past 50 years or so. For example, Wang and Hopkins [1] and Symmonds [2] analyzed the response of clamped circular plates and beams, respectively, under impulsive loads. However, their analyses was restricted to small deflections and linear bending kinematics. By direct application of the principle of virtual work for an assumed deformation mode, Jones presented approximate solutions for simply supported and clamped beams, [3], and also simply supported circular plates, [4], undergoing finite deflections.

Recently, Xue and Hutchinson [5] carried out a preliminary finite element (FE) investigation of the resistance of clamped circular sandwich plates with a foamlike core to shock loading with the effects of fluid-structure interaction neglected. By employing a series of FE calculations they demonstrated that near-optimized circular sandwich plates offer a higher resistance to shock loading than monolithic plates of the same mass. In parallel studies, Fleck and Deshpande [6] proposed an analytical model for the response of clamped sandwich beams to shock loadings including the effects of fluid-structure interaction and showed that the analytical predictions are in close agreement with FE calculations, [7].

In this study we extend the analytical method of Fleck and

Deshpande [6] to clamped circular sandwich plates. First, analytical formulas are presented for the response of clamped rigid-ideally plastic circular sandwich plates to a uniform shock wave, including the effects of fluid-structure interaction. Next, the analytical predictions of the response of sandwich plates are compared with FE predictions for the case where the effect of fluid-structure interaction is neglected: This loading represents shock loading in air. Finally, the analytical formulas are used to determine the optimal designs of sandwich plates that maximize the shock resistance in air for a given mass and the performance gain of these optimal sandwich plates over monolithic plates is quantified.

2 An Analytical Model for the Shock Resistance of Clamped Sandwich Plates

Fleck and Deshpande [6] have developed an analytical model for the response of clamped sandwich beams subject to air and underwater shock loading. This model is now extended to analyze the response of clamped axisymmetric sandwich plates to a spatially uniform air or underwater shock.

Consider a clamped circular sandwich plate of radius R with identical face-sheets of thickness h and a core of thickness c, as shown in Fig. 1. The face-sheets are made from a rigid ideally plastic solid of yield strength σ_{fY}, density ρ_f, and tensile failure strain ϵ_f. The core is taken to be a compressible isotropic solid of density ρ_f and deforms in uniaxial compression the core at a constant strength σ_c with no lateral expansion up to a densification strain ϵ_D; beyond densification the core is treated as rigid. Fleck and Deshpande [6] split the response of the sandwich structure into three sequential stages:

(i)   Stage I—fluid-structure interaction phase,
(ii)   Stage II—core compression phase, and
(iii)   Stage III—plate bending and stretching phase.

Here, we assume a similar separation of time scales for the sandwich plate deformation history.

Stage I—The initial fluid-structure interaction phase

G. I. Taylor [8] developed the solution for a one-dimensional wave impinging a free-standing plate to compute the momentum transmitted to the plate by the shock pulse. Fleck and Deshpande [6] followed this approach and similarly computed the momentum transmitted to the sandwich beam by treating the outer face of the
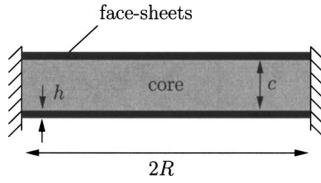

Fig. 1 Geometry of the clamped sandwich plate

sandwich beam as a free-standing plate. Their analysis also holds for the circular sandwich plate, and we briefly review the relevant equations.

The pressure p at any point in the fluid of density ρ_w engulfed by the pressure wave travelling at a velocity c_w is taken to be (starting at time $t=0$)

$$p=p_o e^{-t/\theta},\qquad(1)$$

where p_o is the peak pressure and θ the decay constant of the wave. When this pressure wave hits a stationary rigid plate at normal incidence it imparts an impulse I

$$I=2\int_0^\infty p_o e^{-t/\theta}dt=2p_o\theta,\qquad(2)$$

to the plate. The factor of two arises in relation (2) due to full reflection of the pressure wave.

If instead, the pressure wave impacts a free-standing plate, the imparted impulse is less than I, and can be estimated as follows. When the pressure wave strikes a free-standing plate of thickness h made from a material of density ρ_f, it sets the plate in motion and is partly reflected. At the instant the plate achieves its maximum velocity, the pressure at the interface between the plate and the fluid is zero and cavitation sets in shortly thereafter. The momentum per unit area I_{trans} transmitted into the structure is then given by

$$I_{\text{trans}}=\zeta I,\qquad(3a)$$

where

$$\zeta\equiv\psi^{\psi/(1-\psi)},\qquad(3b)$$

and $\psi\equiv\rho_w c_w\theta/(\rho_f h)$. It is assumed that this transmitted impulse imparts a uniform velocity $v_o=I_{\text{trans}}/(\rho_f h)$ to the outer front face of the sandwich plate.

In the present model, the effect of the fluid after the first cavitation event is neglected. This is consistent with the observation that the secondary shocks have a much smaller effect on the structure compared to the primary shock wave, see Cole [9].

Stage II—Core compression phase

At the start of this phase, the outer face has a velocity v_o while the core and inner face are stationary. The outer face compresses the core, while the core with compressive strength σ_c decelerates the outer face and simultaneously accelerates the inner face. The final common velocity of the faces and the core is dictated by momentum conservation and the ratio ϕ of the energy lost U_{lost} in this phase to the initial kinetic energy $I^2\zeta^2/2\rho_f h$ of the outer face is given by

$$\phi\equiv\frac{U_{\text{lost}}}{I^2\zeta^2/(2\rho_f h)}=\frac{1+\bar m}{2+\bar m},\qquad(4)$$

where $\bar m=\rho_c c/(\rho_f h)$ is the ratio of the mass of the core to the mass of a face-sheet. This energy lost is dissipated by plastic dissipation in compressing the core and thus the average through-thickness strain ϵ_c in the core is given by

$$\epsilon_c=\frac{\bar I^2\zeta^2}{2\bar\sigma\bar c^2\bar h}\frac{\bar h+\bar\rho}{2\bar h+\bar\rho},\qquad(5)$$

where $\bar h\equiv h/c$, $\bar c\equiv c/R$, $\bar\rho\equiv\rho_c/\rho_f$, $\bar I\equiv I/(R\sqrt{\sigma_{fY}\rho_f})$ and $\bar\sigma\equiv\sigma_c/\sigma_{fY}$. However, if U_{lost} is too high such that ϵ_c as given by (5) exceeds the densification strain ϵ_D, then ϵ_c is set equal to ϵ_D and the model does not account explicitly for the additional dissipation mechanisms required to conserve energy. Rather it is assumed that inelastic impact of the outer face against the combined core and inner face leads to the additional dissipation. After the core has compressed by a strain of ϵ_c, the core height is reduced to $(1-\epsilon_c)c$. An approximate estimate of the time T_c for this second stage of motion (calculated by neglecting the mass of the core) is given by [6]

$$\bar T_c\equiv\frac{T_c}{R\sqrt{\rho_f/\sigma_{fY}}}$$

$$=\begin{cases}\dfrac{\bar I\zeta}{2\bar\sigma}, & \text{if }\bar I^2\zeta^2<4\bar\sigma\bar c^2\bar h\epsilon_D\\[2ex]\dfrac{\bar I\zeta}{2\bar\sigma}\left[1-\sqrt{1-\dfrac{4\bar\sigma\bar c^2\bar h\epsilon_D}{\bar I^2\zeta^2}}\right], & \text{otherwise.}\end{cases}$$

$$(6)$$

This time T_c is typically small compared to the structural response time and thus the transverse deflection of the inner face of the sandwich plate can be neglected in this stage.

Stage III—Plate bending and stretching phase

At the end of Stage II, the sandwich plate has a uniform velocity except for a boundary layer near the supports. The plate is brought to rest by plastic bending and stretching. The problem under consideration is a classical one: what is the dynamic response of a clamped plate of radius R with an initial uniform transverse velocity v? The structural response is broken down into two phases: (i) *small displacement analysis* as first considered by Wang and Hopkins [1] and (ii) *large displacement analysis*.

(i) Small displacement analysis

When the transverse displacement of the plate $w(t)$ is less than the total thickness $2h+c$, the dynamic response is governed by bending and transverse inertia of the plate. Wang and Hopkins [1] showed that the plate response comprises two sequential phases. Phase I comprises stationary plastic hinges at the supports and plastic hinges travelling inwards from each clamped support. After the moving hinges have coalesced at the center of the plate, continued rotation occurs about the central hinge until the plate is brought to rest in phase II.

We now introduce the appropriate nondimensional geometric parameters for the sandwich plate

$$\bar c\equiv\frac{c}{R},\quad\hat c\equiv\bar c(1-\epsilon_c),\quad\bar h\equiv\frac{h}{c}\text{ and }\hat h\equiv\frac{\bar h}{1-\epsilon_c},\qquad(7)$$

and the nondimensional material properties of the core

$$\bar\rho\equiv\frac{\rho_c}{\rho_f},\quad\text{and }\bar\sigma\equiv\frac{\sigma_c}{\sigma_{fY}}.\qquad(8)$$

The nondimensional structural response time $\bar T$ and blast impulse $\bar I$ are

$$\bar T\equiv\frac{T}{R}\sqrt{\frac{\sigma_{fY}}{\rho_f}},\quad\bar I\equiv\frac{I}{R\sqrt{\rho_f\sigma_{fY}}}.\qquad(9)$$

In the small deflection regime, the maximum central deflection w of the inner face of the sandwich plate and the structural response time T are given by Eqs. (4.99) and (4.100), respectively, of Jones [4]. Noting that the plastic bending moment M_o of the circular sandwich plate is given by

$$M_o=\sigma_c\frac{(1-\epsilon_c)^2 c^2}{4}+\sigma_{fY}h[(1-\epsilon_c)c+h],\qquad(10)$$

these equations reduce to

$$\bar{w} \equiv \frac{w}{R} = 0.28 \frac{\bar{I}^2 \zeta^2}{\bar{c}\hat{c}^2 \alpha_1 (2\bar{h} + \bar{\rho})}, \qquad (11a)$$

and

$$\bar{T} \equiv \frac{T}{R}\sqrt{\frac{\sigma_{fY}}{\rho_f}} = 0.36 \frac{\bar{I}\zeta}{\hat{c}^2 \alpha_1}, \qquad (11b)$$

where

$$\alpha_1 = (1 + 2\bar{h})^2 - 1 + \bar{\sigma}, \qquad (12a)$$

and

$$\alpha_2 = \sqrt{\frac{2\bar{h} + \bar{\rho}}{2\hat{h} + \bar{\sigma}}}. \qquad (12b)$$

(ii) Large displacement analysis

The above analysis ignores the buildup of membrane action associated with the lateral deflection of the clamped plates. Jones [4] has taken this into account by assuming that the plate deflects from the initial undeformed configuration with a velocity profile which decreases linearly from a maximum value at the center to zero at the supports. The analysis in Jones [4] is given for a simply supported circular plate and can be easily extended to clamped circular plates by assuming that stationary plastic hinges form at the center and at the clamped supports of the plate. Plastic dissipation is both by rotation about discrete plastic hinges and by uniform radial stretching of the plate due to its transverse displacement between the clamped supports.

The yield locus of an axisymmetric sandwich element subjected to a circumferential membrane force N_θ and a circumferential bending moment M_θ is well approximated by

$$\frac{M_\theta}{M_o} + \frac{N_\theta}{N_o} = 1, \qquad (13)$$

where M_o is the plastic bending moment specified by (10) and N_o the circumferential plastic membrane force given by

$$N_o = 2h\sigma_{fY} + (1 - \epsilon_c)c\sigma_c, \qquad (14)$$

where we have assumed the strength of the foam is unaffected by core compression. Analytical formulas for the deflection and structural response time of the circular plate can be obtained by approximating the above yield locus by either inscribing or circumscribing squares as sketched in Fig. 2(a). Employing a procedure similar to that detailed in Jones [4] the maximum central deflection w of the inner face and structural response time T of a clamped circular sandwich plate are given by

$$\bar{w} = \frac{\bar{c}\alpha_1}{2\hat{h} + \bar{\sigma}}\left(\sqrt{1 + \frac{2}{3}\frac{\bar{I}^2 \zeta^2}{\bar{c}\hat{c}^3 \alpha_1^2 \alpha_2^2}} - 1\right), \qquad (15a)$$

and

$$\bar{T} = \alpha_2 \sqrt{\frac{\bar{c}}{6\hat{c}}}\tan^{-1}\left(\sqrt{\frac{2}{3\bar{c}\hat{c}}}\frac{\bar{I}\zeta}{\hat{c}\alpha_1 \alpha_2}\right), \qquad (15b)$$

respectively, for the choice of a circumscribing yield locus, and by

$$\bar{w} = \frac{\hat{c}\alpha_1}{2\hat{h} + \bar{\sigma}}\left(\sqrt{1 + \frac{4}{3}\frac{\bar{I}^2 \zeta^2}{\bar{c}\hat{c}^3 \alpha_1^2 \alpha_2^2}} - 1\right), \qquad (16a)$$

and

$$\bar{T} = \alpha_2 \sqrt{\frac{\bar{c}}{3\hat{c}}}\tan^{-1}\left(\frac{2}{\sqrt{3\bar{c}\hat{c}}}\frac{\bar{I}\zeta}{\hat{c}\alpha_1 \alpha_2}\right), \qquad (16b)$$
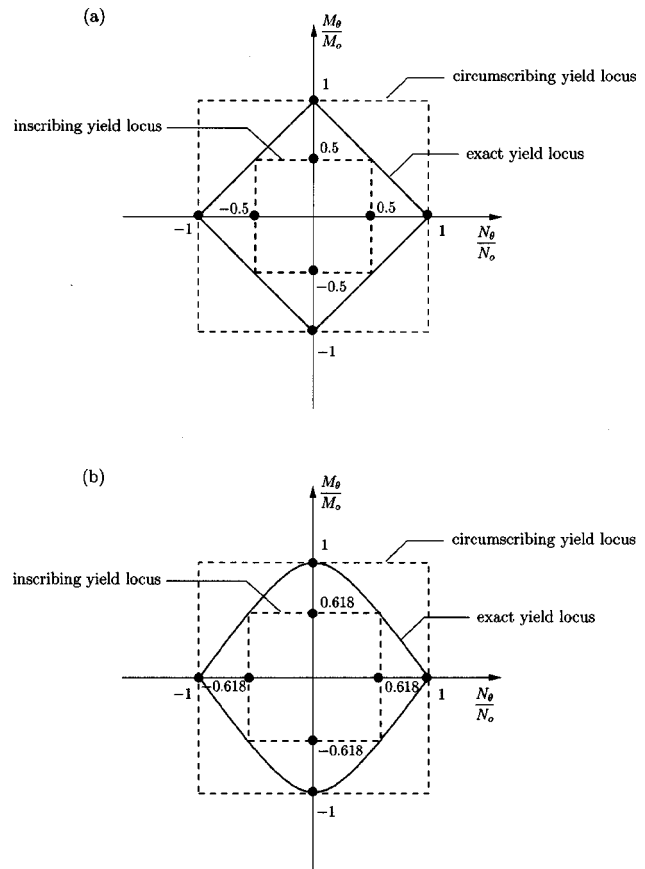

Fig. 2 Sketches of the exact, inscribing and circumscribing yield loci of (*a*) the sandwich plate and (*b*) the monolithic plate. Here, M_o and N_o are the fully plastic bending moments and axial loads, respectively, of the plates.

for an inscribing yield locus. A number of criteria can be devised for the transition from the small to the large deflection analysis. For example, the transition can be assumed to occur at an impulse level where both analyses predict equal displacements. It will be shown subsequently in the comparisons with the FE calculations that for most practical values of displacement or impulses, the large displacement solution suffices. Thus, we propose here to use the large displacement solution over the entire range of impulses.

The circumferential tensile strain ϵ_m in the face-sheets due to stretching is approximately equal to

$$\epsilon_m = \frac{1}{2}\bar{w}^2. \qquad (17)$$

Neglecting the strains due to bending, an approximate failure criterion for the sandwich plates is given by setting the face-sheet tensile strain ϵ_m equal to the tensile ductility ϵ_f of the face-sheet material.

2.1 Response of a Monolithic Clamped Plate. Similar expressions exist for the deflection and structural response time of a monolithic clamped circular plate. For monolithic plates, no core compression phase exists and Stage II of the deformation history vanishes. Again the analysis is divided into the small and large displacement regimes. Consider a monolithic plate of thickness H and radius R made from a solid material with yield strength σ_{fY}. Then the analysis of Wang and Hopkins [1] implies that the maximum central deflection w and the time T to attain this deflection are given by

$$\bar{w} \equiv \frac{w}{R} = 0.28 \bar{I}^2 \zeta^2 \left(\frac{R}{H}\right)^3, \qquad (18a)$$

and

$$\bar{T} \equiv \frac{T}{R} \sqrt{\frac{\sigma_{fY}}{\rho_f}} = 0.36 \bar{I} \zeta \left(\frac{R}{H}\right)^2. \tag{18b}$$

Next consider the large displacement regime. The yield locus for any plate element of the monolithic circular plate, subject to a circumferential membrane force N_θ and bending moment M_θ is given by

$$\left(\frac{M_\theta}{M_o}\right)^2 + \frac{N_\theta}{N_o} = 1, \tag{19}$$

where $N_o = H \sigma_{fY}$ and $M_o = \sigma_{fY} H^2/4$. The maximum central deflection w of the clamped circular plate and the structural response time in the large displacement regime can be calculated in the manner detailed in Jones [4] by approximating the yield locus by either inscribing or circumscribing squares as sketched in Fig. 2(b). Under the assumption of an inscribing yield locus, the nondimensional deflection $\bar{w}$ and structural response time $\bar{T}$ are given by

$$\bar{w} = \left(\frac{H}{R}\right) \left(\sqrt{1 + 1.079 \bar{T}^2 \zeta^2 \left(\frac{R}{H}\right)^4} - 1 \right), \tag{20a}$$

and

$$\bar{T} = 0.519 \tan^{-1} \left[1.039 \bar{I} \zeta \left(\frac{R}{H}\right)^2 \right]. \tag{20b}$$

Similarly, the assumption of a circumscribing yield locus gives

$$\bar{w} = \left(\frac{H}{R}\right) \left(\sqrt{1 + \frac{2}{3} \bar{T}^2 \zeta^2 \left(\frac{R}{H}\right)^4} - 1 \right), \tag{21a}$$

and

$$\bar{T} = \frac{1}{\sqrt{6}} \tan^{-1} \left[\sqrt{\frac{2}{3}} \bar{I} \zeta \left(\frac{R}{H}\right)^2 \right]. \tag{21b}$$

Again, it will be shown via FE calculations that the large displacement solution is adequate over the entire range of deflections.

In the analytical formulas given above, we have ignored shear deflections of the plates. For the slender sandwich plate face-sheets ($h/R \rightarrow 0$) and monolithic plates ($H/R \rightarrow 0$) under consideration here, Jones and Gomes de Oliveira [10] have shown that the shear deflections are negligible. Thus, it suffices to consider only the bending deflections of the plates as done above. Also, strain-rate effects in the parent material have been neglected in the current analysis. As a first-order approximation, Perrone and Bhadra [11] have shown that the effect of strain rate sensitivity can be captured by replacing σ_{fY} with the flow stress σ_o associated with the strain-rate in the beam at the representative transverse deflection $2w/3$.

3 Finite Element Study

In order to assess the accuracy of the above analytical model, a finite element (FE) study was conducted with the effects of fluid-structure interaction neglected. In the limit of no fluid-structure interaction ($\psi = 0$ and $\zeta = 1$) it is assumed that the entire shock impulse I is transferred uniformly to the outer face of the sandwich plate and to the full section of the monolithic plate. It is worth mentioning here that Xue and Hutchinson [5] demonstrated that impulsive loading of clamped circular sandwich plates suffices to capture the response of these plates subject to pressure versus time histories corresponding to most practical shock loadings.

In all the FE calculations presented here, loading corresponding to a nondimensional impulse $\bar{I}$ is specified by imparting an initial uniform velocity v_o

$$v_o = \frac{\bar{I}}{\bar{c}\bar{h}} \sqrt{\frac{\sigma_{fY}}{\rho_f}}, \tag{22}$$

to the outer face-sheet of the sandwich plate and by giving an initial velocity

$$v_o = \frac{\bar{I}R}{H} \sqrt{\frac{\sigma_{fY}}{\rho_f}} \tag{23}$$

uniformly to the monolithic plate.

3.1 Constitutive Description. Unless otherwise specified, the material properties of the sandwich plates are taken to be as follows. The face-sheets of the sandwich plate are assumed to be made from an elastic ideally plastic solid with yield strength σ_{fY}, a yield strain ϵ_{fY} and density ρ_f. The Young's modulus is specified by $E_f \equiv \sigma_{fY}/\epsilon_{fY}$. The solid is modeled as a J2 flow theory solid. The core is modeled as a compressible continuum using the foam constitutive model of Deshpande and Fleck [12]. This constitutive law employs an isotropic yield surface specified by

$$\hat{\sigma} - \sigma_c = 0, \tag{24a}$$

where the equivalent stress is defined by

$$\hat{\sigma}^2 \equiv \frac{1}{1 + (\alpha/3)^2} [\sigma_e^2 + \alpha^2 \sigma_m^2]. \tag{24b}$$

Here, $\sigma_e \equiv \sqrt{3 s_{ij} s_{ij}/2}$ is the von Mises effective stress with s_{ij} the deviatoric stress tensor and $\sigma_m \equiv \sigma_{kk}/3$ the mean stress. The yield strength σ_c is specified as a function of the equivalent plastic strain using uniaxial compression stress versus strain data. Normality of plastic flow is assumed, and this implies that the "plastic Poisson's ratio" $\nu_p = -\dot{\epsilon}_{22}^p/\dot{\epsilon}_{11}^p$ for uniaxial compression in the 1-direction is given by

$$\nu_p = \frac{1/2 - (\alpha/3)^2}{1 + (\alpha/3)^2}. \tag{25}$$

Numerical values for the reference material properties for the sandwich plate were taken to be as follows. The face-sheets are assumed to be made from a stainless steel of yield strength $\sigma_{fY} = 500$ MPa, yield strain $\epsilon_{fY} = 0.2\%$, elastic Poisson's ratio $\nu = 0.3$, and density $\rho_f = 8000$ kgm^{-3}. The strength of the core is taken to be representative of that for a lattice material such as the octet truss, [13], made from the same solid material as the face-sheets. Thus, the isotropic core yield strength is taken to be

$$\sigma_c = 0.5 \bar{\rho} \sigma_{fY}, \tag{26}$$

where $\bar{\rho} \equiv \rho_c/\rho_f$ is the relative density of the core. As the reference case, we take $\bar{\rho} = 0.1$ (i.e., core density $\rho_c = 800$ kgm^{-3}) with $\alpha = 3/\sqrt{2}$ giving a plastic Poisson's ratio $\nu_p = 0$. The plastic crush strength σ_c of the foam core is taken to be independent of the effective plastic strain up to a densification strain $\epsilon_D = 0.5$: beyond densification, a linear hardening behavior is assumed with a very large tangent modulus $E_t = 0.2 E_f$. Further, the core is taken to be elastically isotropic with a yield strain $\epsilon_{cY} = 0.2\%$ and an elastic Poisson's ratio $\nu_c = 0$.

3.2 Details on the Finite Element Method. All computations were performed using the explicit time integration version of the commercially available finite element code ABAQUS version 6.2. The plate was modeled using four-noded axisymmetric quadrilateral elements with reduced integration, (element type $CAX4R$ in the ABAQUS notation). Numerical damping associated with volumetric straining in ABAQUS explicit was switched off by setting the bulk viscosity associated with this damping to zero; using the default viscosity in ABAQUS results in substantial artificial viscous dissipation due to the large volumetric compression of the core. For a typical plate of geometry $\bar{c} = 0.03$ and $\bar{h} = 0.1$, there were 2 and 8 elements through the thickness of the face-sheets and core, respectively, and 100 elements along the radius R.
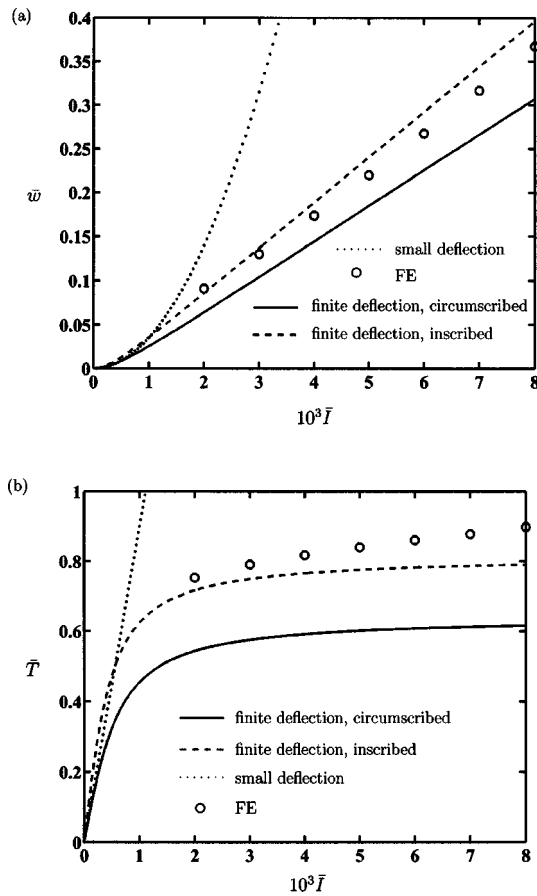
Fig. 3 Analytical and FE predictions of (*a*) maximum central deflection and (*b*) structural response time, of a monolithic plate with aspect ratio $R/H=50$ as a function of the applied impulse
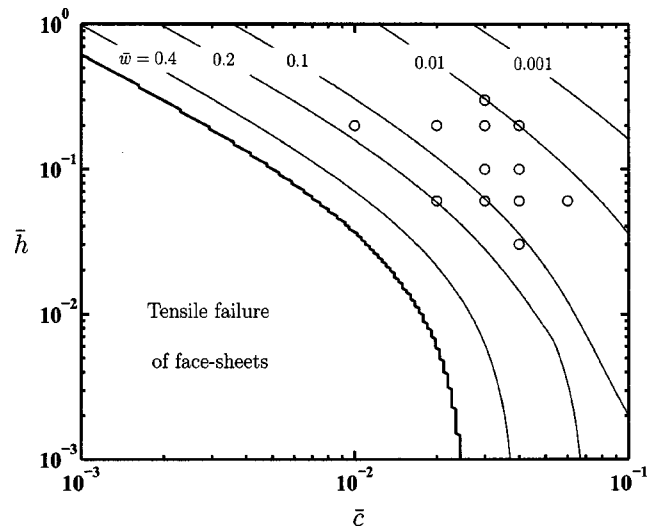

Fig. 4 Design chart for a clamped sandwich plate with core strength $\bar{\sigma}=0.05$ and densification strain $\epsilon_D=0.5$ and an assumed face-sheet material ductility $\epsilon_f=0.2$. Contours of the maximum normalized central deflection $\bar{w}$ of the inner face-sheet subject to a normalized impulse $\bar{I}=10^{-3}$ are included. The symbols denote the sandwich plate geometries selected for the FE calculations.

Mesh sensitivity studies revealed that further refinements did not improve the accuracy of the calculations appreciably.

4 Comparison of Finite Element and Analytical Predictions

4.1 Monolithic Plates. Comparisons between analytical and FE predictions of the dynamic response of monolithic plates made from the same material as the face-sheets of the reference sandwich plate (i.e., an elastic perfectly plastic solid with a yield strength $\sigma_{fY}=500$ MPa, yield strain $\epsilon_{fY}=0.2\%$, an elastic Poisson's ratio $\nu=0.3$ and a material density $\rho_f=8000$ kgm^{-3}) are presented in this section. The dependence of the normalized maximum central deflection $\bar{w}$ of the plate upon the uniformly applied normalized impulse $\bar{I}$ is shown in Fig. 3(*a*), for a plate with aspect ratio $R/H=50$. In the FE simulations, w is defined as the peak value of the central deflection versus time trace. Analytical predictions of this maximum deflection employing the small deflection analysis and the finite deflections analyses with the circumscribing and inscribing yield surfaces are included in Fig. 3(*a*). While the inscribing yield surface predictions are in good agreement with the FE results over the range of impulses investigated here, the circumscribing yield surface model underpredicts the deflections. Further, for realistic levels of the shock impulse, the FE results are captured accurately with the finite deflection analysis employing the inscribing yield locus.

The analytical and FE predictions of the normalized structural response time $\bar{T}$, as functions of the applied normalized impulse $\bar{I}$

are given in Fig. 3(*b*). In the FE simulations, T is defined as the time taken to reach the maximum deflection and written in non-dimensional form via (9). For the range of impulses considered here, the response of the plate is governed by stretching and the structural response time is approximately independent of magnitude of the impulse. It is seen that the FE predictions of the structural response time T are also in good agreement with the analytical model employing the inscribing yield locus. Again the small deflection analysis is not relevant for realistic levels of shock impulses. Thus, in the subsequent discussion we only present comparisons with the finite deflection solution and neglect the small deflection analysis.

4.2 Sandwich Plates. Comparisons of dynamic finite element simulations and analytical predictions have been performed on sandwich plates made from the reference materials specified above. The comparisons between the analytical and FE predictions are carried out in two stages. First, for a fixed impulse, the response of the sandwich plate is investigated as function of the plate geometry and second, the response of a sandwich plate with a representative geometry is studied for varying levels of impulse.

For the purposes of selecting appropriate sandwich plate geometries for the FE calculations, we plot a design chart for sandwich plates subjected to a normalized impulse $\bar{I}=10^{-3}$, with an assumed face-sheet material ductility $\epsilon_f=0.2$. The design chart shown in Fig. 4 has been constructed using the analytical model with the circumscribing yield locus. Contours of the maximum normalized central deflection $\bar{w}$ of the inner face of the sandwich plates along with the regime of tensile failure of the face-sheet are shown on the chart. Twelve plate geometries in the range $0.03 \leqslant \bar{h} \leqslant 0.3$ and $0.01 \leqslant \bar{c} \leqslant 0.06$ (as indicated in Fig. 4) are selected for the FE calculations. This range of plate geometries is representative of practical plate geometries, and the analytic predictions for the central displacements of the inner face of the sandwich plate are in the range $0.01 \leqslant \bar{w} \leqslant 0.2$.

Comparisons of the FE and analytical predictions (inscribing yield locus) for the central deflection $\bar{w}$ of the inner face-sheet as functions of $\bar{h}$ are shown in Fig. 5(*a*) for $\bar{c}=0.03$ and $\bar{c}=0.04$, subject to $\bar{I}=10^{-3}$. Similar to the monolithic beam case, in the FE simulations w is defined as the peak value of the deflection versus time trace. Figure 5(*b*) shows comparisons of the analytical
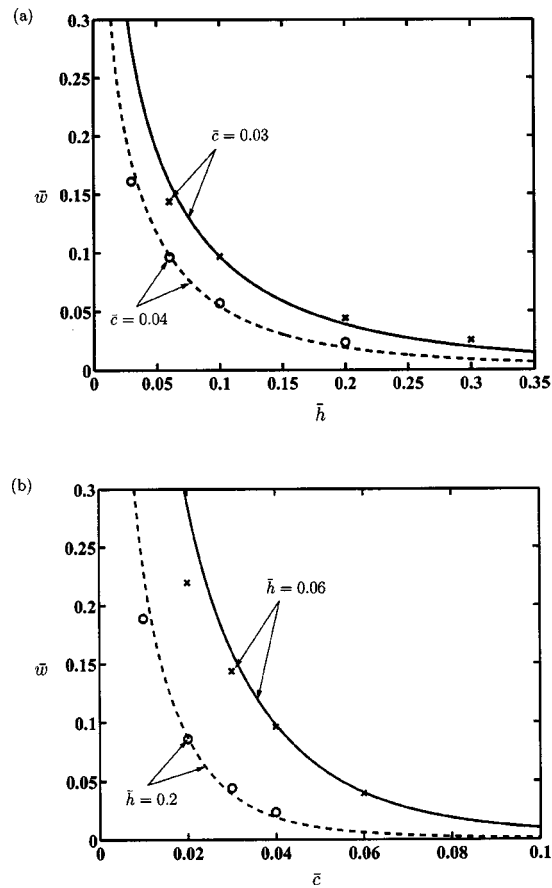
Fig. 5 Analytical and FE predictions of the maximum central deflection $\bar{w}$ of the inner face-sheet of sandwich plates with reference material properties subjected to a normalized impulse $\bar{I}=10^{-3}$. (a) $\bar{w}$ as a function of $\bar{h}$ for two values of $\bar{c}$. (b) $\bar{w}$ as a function of $\bar{c}$ for two values of $\bar{h}$.

Fig. 6 Analytical and FE predictions of the (a) maximum central deflection $\bar{w}$ of the inner face-sheet and (b) core compression ϵ_c as a function of the applied impulse for sandwich plates. $\bar{c}=0.03$ and $\bar{h}=0.1$ and the sandwich plate is made from the reference core material, with both ideally plastic and strain hardening face-sheets.

and FE predictions of $\bar{w}$ versus $\bar{c}$ for plates with $\bar{h}=0.06$ and 0.2, again for the fixed impulse $\bar{I}=10^{-3}$. In all of the above cases good agreement is seen between the analytical and FE predictions, with the discrepancy in w between the analytical and FE predictions not exceeding 5%. As in the monolithic plate case, the analytical model employing the circumscribing yield locus underpredicts the deflections.

Next consider a representative sandwich plate of geometry, $\bar{c}=0.03$ and $\bar{h}=0.1$, subject to impulses in the range $7.5\times10^{-4}\leqslant\bar{I}\leqslant3.2\times10^{-3}$. A comparison of the FE and analytical predictions of the maximum deflection $\bar{w}$ and core compression ϵ_c versus $\bar{I}$ are shown in Figs. 6(a) and 6(b), respectively. In the FE simulations, the strain ϵ_c is defined as the final through thickness nominal strain at the center of the plate. The choice of an inscribing yield surface for the analytical model leads to good agreement with the finite element predictions at low impulses, while at higher impulses the circumscribing yield surface appears to give better predictions. Figure 6(b) shows that the analytical calculation also substantially overpredicts the core compression in the high impulse domain. Similar to the sandwich beam case analyzed in Qiu et al. [7], these discrepancies can be rationalized by recalling that the analytical model neglects the reduction in momentum due to an impulse provided by the supports in the core compression phase. With increasing impulse this assumption is no longer valid as the higher core compression gives rise to significant stretching of the outer face-sheet at the supports and thus to a loss in momentum. This effect is not accounted for in the analytical
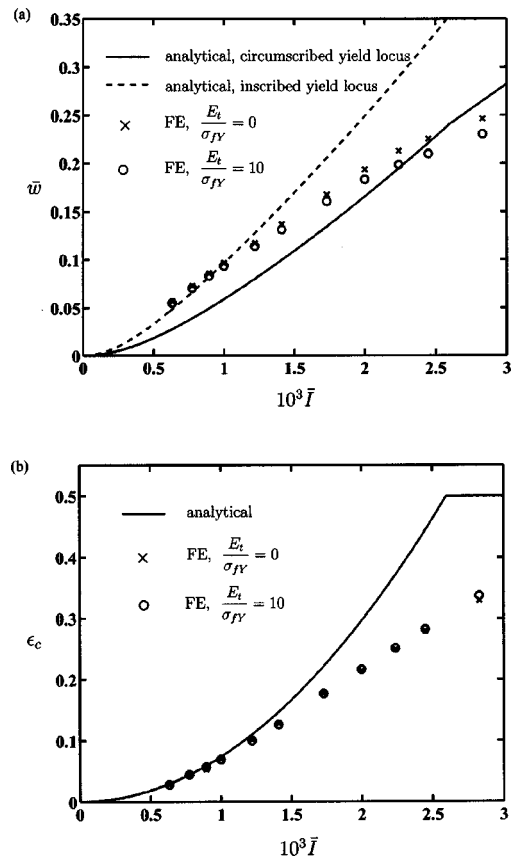
model and consequently the analytical model overpredicts the deflections and core compression at high values of impulse.

In the FE simulations, the structural response time T is defined as the time taken to reach the maximum deflection and the core compression time T_c is defined as the time taken to first attain the final through thickness strain ϵ_c in the core. Comparisons of the analytical and FE predictions of the normalized structural response time $\bar{T}$ and the core compression time $\bar{T}_c$ as functions of $\bar{I}$ are shown in Fig. 7 for the sandwich plate with $\bar{c}=0.03$ and $\bar{h}=0.1$. Good agreement between the analytical and FE predictions is seen for the core compression time and, similar to the case of the monolithic plate, the inscribing yield locus model is in good agreement with the FE predictions of the structural response time. The normalized core compression time $\bar{T}_c$ is at least an order of magnitude smaller than the structural response time $\bar{T}$; this supports the assumption of a separation of time scales for the core compression phase and the plate bending and stretching phase in the analytical model.

4.2.1 Effect of Strain Hardening Upon the Dynamic Response of Sandwich Plates. The analytical models discussed in Section 2 and the FE calculations detailed above, both assume ideally plastic face-sheet materials. On the other hand, structural alloys, which are expected to be employed in shock resistant sandwich construction, can have a strong strain hardening response. The effect of strain hardening of the face-sheet material on the sandwich plate response is investigated here by suitable modifications of the FE model. The face-sheet material is assumed to be made
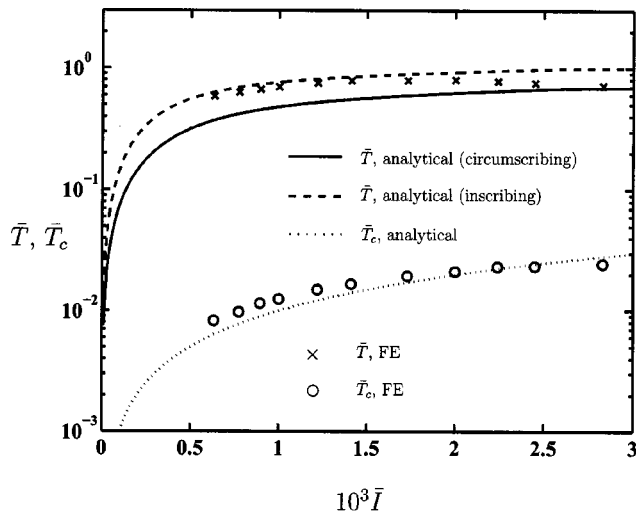
Fig. 7 A comparison between analytical and FE predictions of the structural response time $\bar{T}$ and core compression time $\bar{T}_c$, as a function of the applied impulse, for sandwich plates with $\bar{c} = 0.03$ and $\bar{h} = 0.1$ made from the reference materials

Fig. 8 A comparison between the analytical and FE predictions of the maximum central deflection $\bar{w}$ of the inner face-sheet of sandwich plates with $c = 0.03$ and $\bar{h} = 0:1$, subject to a normalized impulse $I = 10^{-3}$ as a function of the normalized core strength $\bar{\sigma}$

from a elastic plastic material with yield stress and strain $\sigma_{fY} = 500$ MPa and $\epsilon_{fY} = 0.2\%$, respectively, and a density $\rho_f = 8000$ kgm^{-3}. The strain hardening response is assumed to be linear with a tangent modulus $E_t / \sigma_{fY} = 10$; this high rate of strain hardening is representative of the AL6XN stainless steel. The core properties are unchanged from the reference material case.

Consider a sandwich plate with core made from the reference material and elastic strain hardening plastic face-sheets, with geometry $\bar{c} = 0.03$ and $\bar{h} = 0.1$. The normalized maximum deflection $\bar{w}$ and core compression ϵ_c are plotted against $\bar{I}$ in Figs. 6(a) and 6(b), respectively, along with the deflections and core compressions of the sandwich plates made from the reference materials (with elastic-ideally plastic face-sheets). The strain hardening response of the face-sheets has only a small effect upon the deflection and core compression of the sandwich plate. This can be rationalised by recalling that the circumferential strain in the face-sheets is $\epsilon_m \approx 0.5\bar{w}^2 \approx 4.5\%$ for $\bar{w} \approx 0.3$. This level of straining does not increase the yield strength of the face-sheet material appreciably for the strain hardening considered here and hence the response is only mildly sensitive to the strain hardening behavior of the face-sheets. This conclusion should be moderated for the case of annealed face-sheets for which the flow strength at a uniaxial strain of 4.5% may be significantly above the yield strength.

4.2.2 Effect of Core Strength Upon the Dynamic Response of Sandwich Plates. In the calculations detailed above, the core strength was held constant. Here we investigate the effect of core strength on the sandwich plate response. Results are presented for sandwich plates of geometry $\bar{c} = 0.03$ and $\bar{h} = 0.1$, subjected to a normalized impulse $\bar{I} = 10^{-3}$. Other than the core strength, the material properties of the sandwich plates were unchanged from the reference material properties. The normalized core strength $\bar{\sigma}$ was varied from 0.01 to 0.08, with a densification strain ϵ_D held fixed at 0.5; cores weaker than $\bar{\sigma} = 0.01$ were not considered as numerical difficulties were encountered in such cases.

The maximum normalized deflection of the inner face of the sandwich plate $\bar{w}$ is plotted against the normalized core strength $\bar{\sigma}$ in Fig. 8. The FE results indicate that $\bar{w}$ is relatively insensitive to the core strength. Analytical predictions of $\bar{w}$ employing the inscribing and circumscribing yield surfaces are included in Fig. 8; the analytical model employing the inscribing yield surface agrees reasonably well with the FE predictions for plates with the high
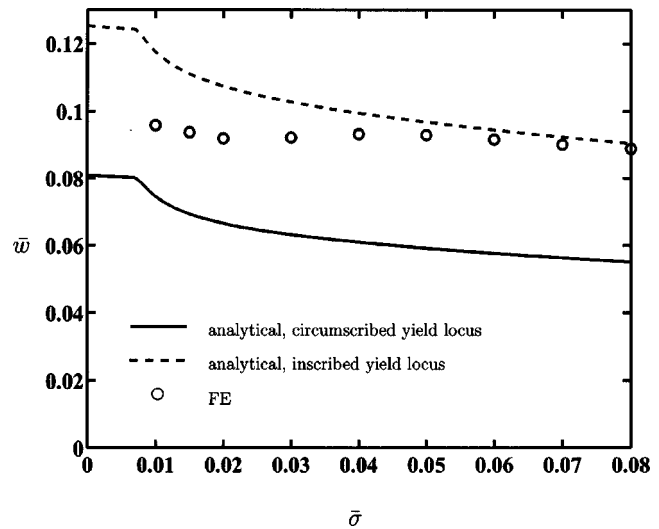
core strength but overpredicts the deflection of the plates with the weaker cores. Time histories of the plastic dissipation of the entire sandwich plate and of the core alone, each normalized by the initial kinetic energy of the outer face-sheet of the sandwich plate are shown in Fig. 9(a). These curves reveal two stages of deformation. In the first stage, plastic dissipation occurs primarily in the core, with the outer face-sheet approaching the inner face; at the end of this stage both face-sheets are moving at approximately the same velocity. Subsequently, plastic dissipation occurs primarily within the face-sheets, with the dissipation in the core increasing only gradually with time. It is worth noting that the plastic dissipation in the core at the end of the first stage is nearly independent of the core strength. Further, this stage lasts longer for the weaker cores. Consequently, the core compression phase overlaps with that for the face-sheet deformation for the choice of a sandwich plate with a weak core.

Finite element predictions of the plastic dissipation at the end of the first stage of the deformation (i.e., the plastic dissipation corresponding up to the "knee" in the plastic dissipation versus times curves of Fig. 9(a)) are shown in Fig. 9(b) as a function of the mass ratio $\bar{m} = \rho_c c / (\rho_f h)$, for the choices of core strength $\bar{\sigma} = 0.04$ and $\bar{\sigma} = 0.01$. These calculations were conducted on plates with the above geometry subject to a normalized impulse $\bar{I} = 10^{-3}$. The ratio $\bar{m}$ was varied by changing the density of the core material from 80 kgm^{-3} to 1600 kgm^{-3}. The figure reveals that the plastic dissipation at the end of the core compression stage is independent of the core strength and increases with $\bar{m}$, in excellent agreement with the analytical predictions, Eq. (4).

4.2.3 Comparison of the Dynamic Response of Clamped Sandwich Plates and Beams. Comparisons between FE and analytical predictions of the impulsive response of clamped sandwich beams have already been presented by Qiu et al. [7]. Here we compare the analytical and FE predictions of the deflection w of sandwich plates with these existing results for sandwich beams.

Consider a clamped sandwich beam of span $2L$ comprising two identical face-sheets of thickness h and a core of thickness c made from the reference materials described above. Qiu et al. [7] presented FE results of the maximum normalized midspan defection $\bar{w} \equiv w/L$ of such sandwich beams with geometry $\bar{c} \equiv c/L = 0.03$ and $\bar{h} \equiv h/c = 0.1$ as a function of the applied normalized impulse $\bar{I} \equiv I/(L\sqrt{\rho_f \sigma_{fY}})$. These results are plotted in Fig. 10 along with the corresponding sandwich plate results. We note that the FE
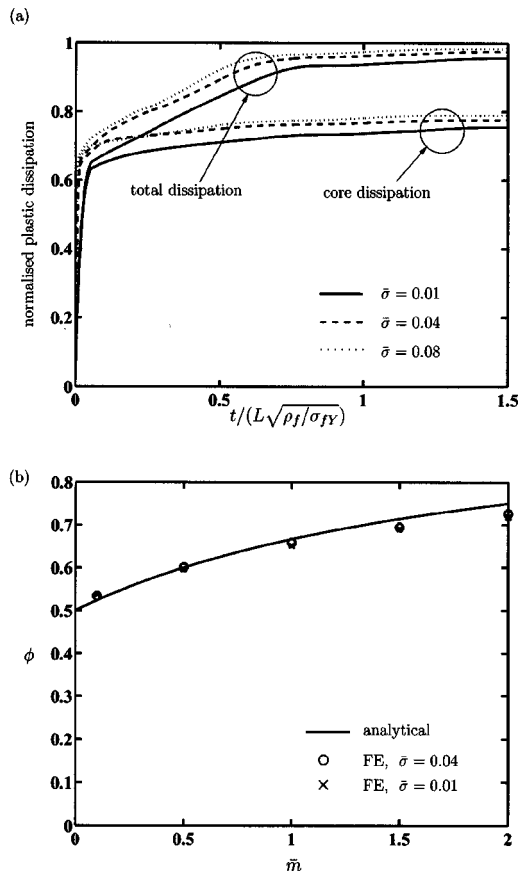
Fig. 11 Design chart for a clamped sandwich plate made from the reference materials for a fixed maximum central deflection of the inner face $\bar{w}=0.1$. Contours of the applied impulse $\bar{I}$ and nondimensional mass $\bar{M}$ are displayed. The underlined values denote the nondimensional impulse values while the arrows trace the path of the optimal designs with increasing $\bar{M}$.

Fig. 9 (a) FE predictions of the time histories of the normalized plastic dissipation in sandwich plates for three selected core strengths. (b) Ratio ϕ of the plastic dissipation in the core compression stage to the initial kinetic energy of the outer face as a function of the mass ratio $\bar{m}$ for two selected core strengths. The sandwich plates in both cases have geometry $\bar{c}=0.03$ and $\bar{h}=0.1$ and are subjected to an impulse $\bar{I}=10^{-3}$.
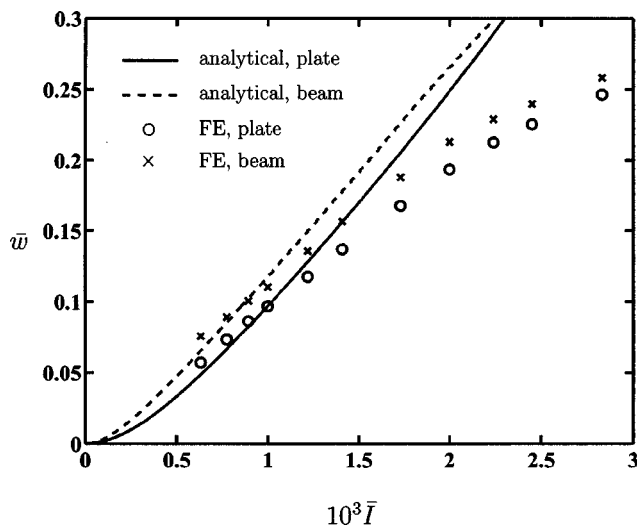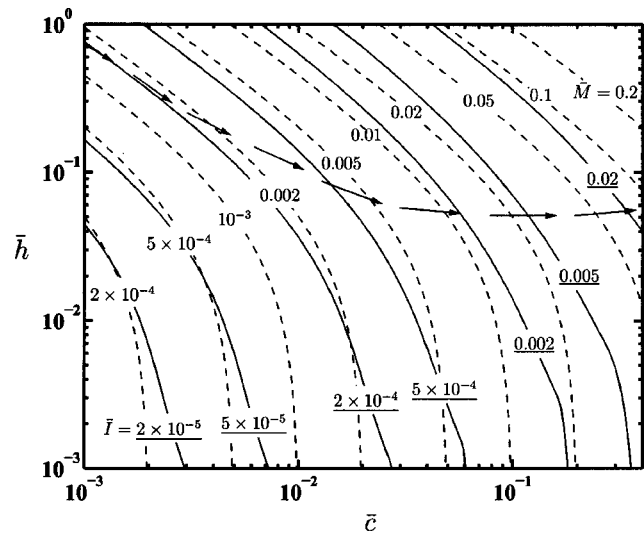

Fig. 10 Analytical and FE predictions of the maximum central deflections $\bar{w}$ of the inner face-sheet for clamped sandwich plates and beams, as a function of the applied impulse. Both the sandwich plates and beams have a geometry $\bar{c}=0.03$ and $\bar{h}=0.1$, and are made from the reference materials.

predictions of the maximum deflections of the clamped sandwich beams and plates as functions of the applied normalized impulse are approximately equal when the half-span L of the sandwich beam is equated to the radius R of the sandwich plate. The analytical predictions (employing the inscribing yield locus) of the deflections of the beams [7] and plates are included in Fig. 10. In line with the FE predictions, the analytical predictions for the beams and plates are approximately equal.

5 Optimal Design of Sandwich Plates Subject to Shock Loading

In the preceding sections we have demonstrated that the finite deflection analytical formulas for the response of the clamped sandwich plates are in reasonable agreement with FE calculations. We now employ these analytical finite deflection formulas to determine the optimal designs of sandwich plates that maximise the resistance of a sandwich plate of given mass to shock loading subject to the constraint of a maximum allowable inner face deflection. The optimization is conducted by assuming that the entire shock impulse is transmitted to the sandwich plate ($\zeta=1$). This is representative of shock loading in air where the acoustic impedance of air is much less than that of the steel outer face-sheet of the sandwich plate as detailed in the Stage I analysis of Section 2.

To help with this optimization, it is instructive to construct a design chart relating the sandwich plate geometry to the shock impulse for a specified deflection. Such a design chart with axes $\bar{c}$ and $\bar{h}$ is plotted in Fig. 11 for a normalized deflection $\bar{w}=0.1$ of the inner face of the sandwich plate by employing the circumscribing yield locus analytical expressions. The chart is plotted for sandwich plates with reference materials properties, i.e., a core of relative density $\bar{\rho}=0.1$ and strength specified by (26). Contours of the nondimensional mass $\bar{M}$ of the sandwich plates have been added to Fig. 11, where

$$\bar{M} \equiv \frac{M}{\pi R^3 \rho_f} = 2\bar{h}\bar{c} + \bar{c}\bar{\rho}, \qquad (27)$$

and M is the mass of the sandwich plate. The arrows in Fig. 11 trace the trajectory of $(\bar{c}, \bar{h})$ which maximizes $\bar{I}$ for a given $\bar{M}$ with increasing $\bar{M}$.
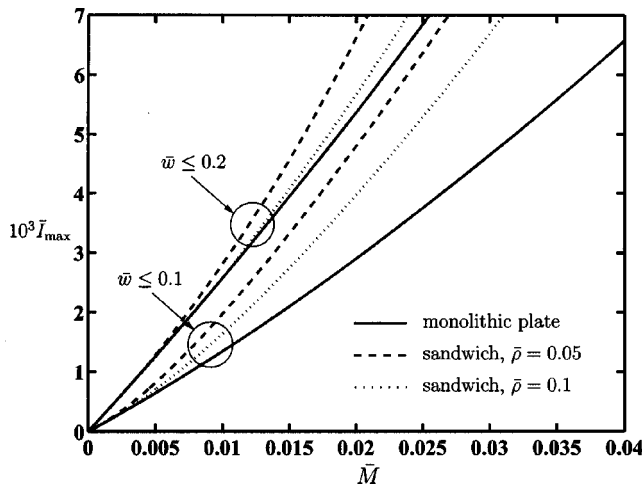
Fig. 12 A comparison of the maximum shock impulse sustained by monolithic plates and by optimal designs of the sandwich plates subject to the constraints $\bar{w}<0.1$ and $\bar{w}\leq0.2$ for two relative densities $\bar{\rho}$ of the core material

The maximum normalized impulse $\bar{I}_{\max}$ sustained by these optimal designs is plotted in Fig. 12 as a function of the nondimensional mass $\bar{M}$. Closed-form expressions for the optimal designs do not exist and hence only numerical results are presented here. Also included in Fig. 12 are the maximum impulses sustained by sandwich plates comprising a core with $\bar{\rho}=0.05$ and strength again specified by (26): Sandwich plates comprising the less dense core have a superior performance. The maximum impulses sustained by the sandwich plates with the constraint on the allowable deflection of the inner face relaxed to $\bar{w}\leq0.2$ are also included in Fig. 12 for the sandwich plates with the $\bar{\rho}=0.05$ and 0.1 cores: the sandwich plates sustain about a 40% higher impulse with the constraint $\bar{w}\leq0.2$ as compared to $\bar{w}\leq0.1$.

For comparison purposes the impulses sustained by monolithic plates made from the same material as the sandwich plate face-sheets and subject to the constraints $\bar{w}\leq0.1$ and $\bar{w}\leq0.2$ are included in Fig. 12 with the choice of the circumscribing yield locus. In the monolithic case the nondimensional mass of the monolithic plates is

$$\bar{M}\equiv\frac{M}{\pi R^{3}\rho_{f}}=\frac{H}{R}, \qquad (28)$$

in terms of the mass M of the monolithic plate. In all cases, the optimal sandwich plates out-perform monolithic plates. However, the performance gain obtained by employing sandwich construction reduces if the maximum allowable deflections $\bar{w}$ are larger: at large deflections the resistance of the plates is primarily due to the stretching action and the performance advantage of the sandwich plates in terms of their high bending resistance plays a much smaller role. It is worth mentioning here that the results will not qualitatively change if the optimisations were performed using the inscribing yield locus instead of the circumscribing yield locus.

6 Conclusions

An analytical model for the response of clamped circular plates subject to shock loading in air and underwater has been derived using the framework proposed by Fleck and Deshpande [6] for clamped sandwich beams. The predictions of the analytical model have been compared with dynamic FE results with the effect of fluid-structure interaction neglected and the analytical model used to determine optimal designs of the sandwich plates. The main findings include:

1. FE calculations demonstrate that the time scale for core compression separates from the time scale for plate bending/stretching of the sandwich plate, as assumed in the analytical model.
2. the analytical model employing the inscribing yield locus agrees well with the FE predictions at small deflections while the FE results are in better agreement with the analytical predictions employing the circumscribing yield locus at larger deflections.
3. for realistic levels of plates deflections, the presence of strain hardening representative that for most structural alloys has a negligible influence on the sandwich plate response.
4. both the FE calculations and the analytical model predict that the compressive strength of the core has only a limited influence on the sandwich plate response.
5. optimal designs of sandwich plates sustain larger shock impulses than monolithic plates of the same mass assuming that the face-sheets of the sandwich plate are made from the same solid as that of the monolithic plate.

References

[1] Wang, A. J., and Hopkins, H. G., 1954, "On the Plastic Deformation of Built-in-Circular Plates Under Impulsive Load," J. Mech. Phys. Solids, **3**, pp. 22–37.
[2] Symmonds, P. S., 1954, "Large Plastic Deformations of Beams Under Blast Type Loading," *Proceedings of the Second US National Congress of Applied Mechanics*, pp. 505–515.
[3] Jones, N., 1971, "A Theoretical Study of the Dynamic Plastic Behavior of Beams and Plates With Finite Deflections," Int. J. Solids Struct., **7**, pp. 1007–1029.
[4] Jones, N., 1989, *Structural Impact*, Cambridge University Press, Cambridge, UK.
[5] Xue, Z., and Hutchinson, J. W., 2003, "A Preliminary Assessment of Sandwich Plates Subject to Blast Loads," Int. J. Mech. Sci., **45**, pp. 687–705.
[6] Fleck, N. A., and Deshpande, V. S., 2004, "The Resistance of Clamped Sandwich Beams to Shock Loading," ASME J. Appl. Mech., **71**, 386–401.
[7] Qiu, X., Deshpande, V. S., and Fleck, N. A., 2003, "Finite Element Analysis of the Dynamic Response of Clamped Sandwich Beams Subject to Shock Loading," Eur. J. Mech. A/Solids, **22**, 801–814.
[8] Taylor, G. I., 1963, *The Scientific Papers of G I Taylor, Vol III*, pages 287–303. Cambridge University Press, Cambridge, UK, pp. 287–303 (The Pressure and Impulse of Submarine Explosion Waves on Plates, 1941).
[9] Cole, R. H., 1948, *Underwater Explosions*, Princeton University Press, Princeton, NJ.
[10] Jones, N., and Gomes de Oliveira, J., 1980, "Dynamic Plastic Response of Circular Plates With Transverse Shear and Rotary Inertia," ASME J. Appl. Mech., **47**, pp. 27–34.
[11] Perrone, N., and Bhadra, P., 1984, "Simplified Large Deflection Mode Solutions for Impulsively Loaded, Viscoplastic, Circular Membranes," ASME J. Appl. Mech., **51**, pp. 505–509.
[12] Deshpande, V. S., and Fleck, N. A., 2000, "Isotropic Constitutive Models for Metallic Foams," J. Mech. Phys. Solids, **48**(6–7), pp. 1253–1283.
[13] Deshpande, V. S., Fleck, N. A., and Ashby, M. F., 2001, "Effective Properties of the Octet-Truss Lattice Material," J. Mech. Phys. Solids, **49**(8), pp. 1747–1769.